Journal of *Marine Science and Engineering*

MDPI

Article

Posterior Probability-Based Symbol Detection Algorithm for CPM in Underwater Acoustic Channels

Ruigang Han [1,2,3], Ning Jia [1,2,3,*], Yufei Liu [1,2,3], Jianchun Huang [1,2,3], Suna Qu [1,2,3] and Shengming Guo [1,2,3]

[1] Institute of Acoustics, Chinese Academy of Sciences, Beijing 100190, China; hanruigang@mail.ioa.ac.cn (R.H.); liuyufei@mail.ioa.ac.cn (Y.L.); huangjianchun@mail.ioa.ac.cn (J.H.); qusuna@mail.ioa.ac.cn (S.Q.); guoshengming@mail.ioa.ac.cn (S.G.)
[2] Key Laboratory of Underwater Acoustic Environment, Chinese Academy of Sciences, Beijing 100190, China
[3] University of Chinese Academy of Sciences, Beijing 100049, China
* Correspondence: jianing@mail.ioa.ac.cn

Abstract: The underwater acoustic (UWA) communication system is characterized by limited bandwidth, while continuous phase modulation (CPM) offers a constant envelope, improving power and spectrum utilization efficiency. However, severe inter-symbol interference (ISI) poses a significant challenge in CPM-based UWA communication. Traditional CPM frequency domain equalization (FDE) combined with simple phase detection neglects the inherent coding gain from CPM, leading to performance degradation. Although Viterbi detection provides high performance, its complexity makes it unsuitable for computationally constrained UWA systems. This paper proposes a symbol detection algorithm based on posterior probabilities combined with FDE (PS-FDE). PS-FDE improves CPM signal detection performance by effectively separating information, applying delay, and performing multiple rounds of information merging. Simulations using minimum shift keying (MSK) and Gaussian MSK signals demonstrate significant performance improvement in just a few iterations over UWA channels. A sea trial further validates the algorithm, showing a 15.83% reduction in bit error rate after three information mergings.

Keywords: underwater acoustic communication; continuous phase modulation; frequency domain equalization; posterior probability-based symbol detection

check for updates

Academic Editor: Lei Wan

Received: 5 March 2025
Revised: 12 April 2025
Accepted: 15 April 2025
Published: 17 April 2025

Citation: Han, R.; Jia, N.; Liu, Y.; Huang, J.; Qu, S.; Guo, S. Posterior Probability-Based Symbol Detection Algorithm for CPM in Underwater Acoustic Channels. *J. Mar. Sci. Eng.* **2025**, *13*, 800. https://doi.org/10.3390/jmse13040800

Copyright: © 2025 by the authors. Licensee MDPI, Basel, Switzerland. This article is an open access article distributed under the terms and conditions of the Creative Commons Attribution (CC BY) license (https://creativecommons.org/licenses/by/4.0/).

1. Introduction

The demand for high-speed underwater acoustic (UWA) communication has progressively intensified in tandem with advancements in marine engineering and technology [1–3]. The conventional phase-shift keying (PSK) modulation scheme faces significant limitations due to the constrained bandwidth of UWA channels and the restricted power output of UWA transducers. Continuous phase modulation (CPM) [4,5], which has found widespread application in aviation telemetry and satellite communications [6–8], offers a compelling alternative. CPM enhances the bandwidth and power efficiency of UWA communication by virtue of its constant envelope, minimal out-of-band radiation, inherent robustness, and intrinsic coding gain.

Among the various wireless communication channels, UWA channels are among the most intricate, leading to substantial signal losses [9,10]. The continuous phase and the nonlinear nature inherent to CPM signals further complicate the design of signal receivers. Ideally, a CPM-modulated signal is detected using the Viterbi algorithm for maximum likelihood sequence estimation, involving a search within a singular super grid [11]. However, the practical realization of this approach is impeded by the algorithm's complexity,

which escalates exponentially with increasing signal length and the varying characteristics of the communication channel. Duel-Hallen and Heegard [12] mitigated this complexity by employing a delayed decision-feedback sequence estimation method. Nevertheless, significant challenges remain, particularly when addressing long-delay spread channel responses with relatively high complexity. Numerous studies have sought to simplify the receiver algorithm by decoupling equalization and detection, as proposed by Laurent [13] and Mengali and Morelli [14], through CPM decomposition. Additionally, minimum mean square error (MMSE)-based suboptimal linear equalization has been applied to counter inter-symbol interference.

Tan and Stuber [15] employed Laurent and orthogonal decompositions to achieve frequency domain equalization (FDE) of CPM signals in frequency-selective fading channels. A straightforward differential detection scheme for CPM signals with a modulation index of $1/2$ was introduced, significantly reducing the complexity of symbol detection. The effectiveness of the algorithm was validated using minimum shift keying (MSK) and Gaussian MSK (GMSK) signals. Pancaldi and Vitetta [16] further advanced the development of minimum mean square error (MMSE) equalization for CPM signals in the frequency domain by implementing linear, decision feedback, and turbo equalization techniques. Additionally, leveraging the inherent characteristics of CPM, they proposed an iterative symbol detection algorithm without channel coding, which was integrated with decision feedback equalization. The binary 3-RC format was adopted for performance verification.

Several research efforts have focused on simplifying the process for CPM signals. Park et al. [17] proposed a simplified decision-feedback equalization scheme, which effectively mitigates the computational complexity associated with the Fourier transform and the Viterbi decoder. Van Thillo et al. [18] approximated the autocorrelation matrix of a CPM signal as a diagonal block matrix, thereby simplifying the MMSE equalization into a low-complexity zero-forcing equalizer, significantly reducing the computational burden of FDE. Building on the insights from these studies, Saleem and Stüber [19] further reduced complexity by simplifying low-energy pulses derived from Laurent decomposition. Chayot et al. [20] leveraged the fractional interval representation of CPM to formulate MMSE-based FDE, which approximates the channel matrix and the pseudo-symbol correlation matrix of the CPM signal. Meanwhile, through the use of shaped-offset quadrature PSK, Rice and Perrins [21] demonstrated that the FDE techniques proposed by Tan and Stüber, Pancaldi and Vitetta, and Van Thillo et al. exhibit comparable performance in weak multipath communication channels.

Numerous studies have explored the integration of channel estimation [22–25] and coding techniques [26,27] to enhance system performance. Van Thillo et al. [22,23] introduced a novel block structure designed to ensure the phase continuity of a single symbol block, replacing the traditional training sequence for channel estimation with a cyclic prefix (CP). This approach reduces transmission information redundancy while maintaining channel estimation performance. Ozgul et al. [26] developed a receiver based on turbo equalization combined with various channel coding methods, though they continued to employ the Viterbi algorithm for symbol detection in CPM signals. While existing FDE algorithms for CPM signals demonstrate effectiveness in frequency-selective fading channels, their application to symbol detection becomes increasingly complex when using the Viterbi algorithm. Furthermore, simple phase detection techniques fail to account for the inherent memory of CPM signals, which leads to a degradation in performance.

This study addresses the issues of high complexity in the Viterbi algorithm and performance loss due to simple phase detection in CPM signal reception by proposing a posterior probability-based symbol detection algorithm based on the CPM symbol detection concept from [16]. The posterior probability-based symbol detection combined with FDE (PS-FDE)

can significantly enhance the reception performance of CPM signals while incurring only a marginal increase in computational complexity. This symbol detection algorithm relies solely on the inherent coding gain of CPM signals and does not depend on additional channel coding. After passing through FDE, the CPM signal obtains the initial likelihood values for each symbol via simple phase detection. Then, based on the characteristics of CPM signals, the contained information is separated, delayed, and merged to obtain the symbol log-likelihood value after the information merging. The estimated log-likelihood value can be used as the initial likelihood value to adjust the weight of information merging. PS-FDE detection, after 2–3 rounds of the information merging, can effectively enhance the reception performance of CPM signals.

The remainder of this paper is organized as follows: Section 2 introduces the system model of CPM UWA communication based on Laurent decomposition that includes the frame structure and preprocessing before PS-FDE; Section 3 describes the proposed algorithm and analyzes the computational complexity; Section 4 presents the numerical simulations used to evaluate the proposed algorithm performance; Section 5 discusses the sea trial performed to verify the proposed algorithms; and Section 6 concludes the paper.

2. System Model

Figure 1 depicts the architecture of the CPM UWA communication system. Preceding CPM, the transmitted data must be added with a tail symbol and CP, containing a unique word. Following CPM signal that passes through the UWA channel, the signal is captured by the receiver, wherein competent time–frequency synchronization and Doppler compensation are assumed to be executed. Subsequently, the received data are extracted through matched filtering, channel equalization, and symbol detection.

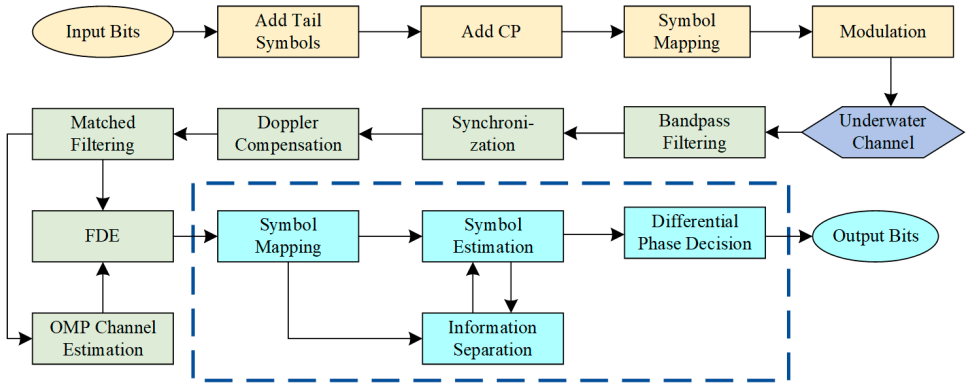

Figure 1. Block diagram of CPM UWA communication system.

2.1. Transmitted Signal

As shown in Figure 2, the transmitted data require a special frame structure for channel equalization. The data bit sequence $\boldsymbol{a} = \{a_{-N_c}, \ldots, a_0, \ldots, a_{N_m-1}, \ldots, a_{N_m-N_t-1}, \ldots, a_{N-N_c-1}\}$ is $N = N_m + N_t + 2 \times N_c$ long, where N_m is the transmitted information length, N_t is the tail symbol length, and N_c is the CP length. CP is used to construct the cyclic matrix for FDE channel estimation. The tail symbol ensures that the phase continuity of the CPM signal is not destroyed after adding CP. The channel estimation algorithm used in this paper is the orthogonal matching pursuit (OMP) algorithm, which is adapted for CPM signals.

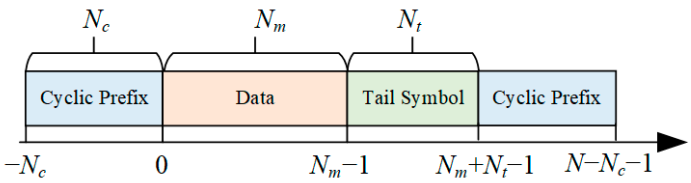

Figure 2. Complete frame structure of the transmitted signal.

According to Laurent decomposition [13], the amplitude-normalized CPM signal is expressed as follows:

$$u(t) = \exp(j\phi(t;\boldsymbol{a})), \tag{1}$$

where the symbols belong to the M-ary alphabet $a_n \in \{\pm 1, \pm 3, \ldots, \pm(M-1)\}$. The excess phase is represented as [13]

$$\phi(t;\boldsymbol{a}) = 2\pi h \sum_{n=-N_c}^{N-N_c-1} a_n q(t-nT), \tag{2}$$

where h is the modulation index, and T is the symbol period. The phase shaping function $q(t)$ is formulated as follows:

$$q(t) = \int_0^t g(\tau)d\tau, \tag{3}$$

where $g(\tau)$ is the frequency-shaping pulse of length LT, and L is defined as the memory length of the CPM signal after Laurent decomposition.

The CPM signal with Laurent decomposition is expressed as the superposition of 2^{L-1} pulse amplitude modulation signals in the following equation [13]:

$$u(t) = \sum_{n=-N_c}^{N-N_c-1} \sum_{p=0}^{2^L-1} \exp(j\pi h \alpha_{n,p}) c_p(t-nT), \tag{4}$$

here

$$c_p(t) = c(t) \prod_{n=1}^{L-1} c(t + (n + L\beta_{n,p})T) \tag{5}$$

and

$$\alpha_{n,p} = \sum_{m=0}^{n} a_m - \sum_{m=1}^{L-1} a_{n-m}\beta_{n,p}. \tag{6}$$

β is the binary representation of p. Then,

$$c(t) = \begin{cases} \frac{\sin(2\pi h q(t))}{\sin \pi h}, & 0 \le t \le LT \\ \frac{\sin(\pi h - 2\pi h q(t-LT))}{\sin \pi h}, & LT \le t \le 2LT \\ 0, & \text{else} \end{cases}. \tag{7}$$

2.2. Received Signal

The transmitted signal passes through the UWA channel. After undergoing time–frequency synchronization and Doppler compensation, the received signal can be mathematically expressed as follows:

$$y(t) = \sum_{\eta=0}^{N_d-1} u(t-\eta T)h_\eta + z(t), \tag{8}$$

where $\boldsymbol{h}$ is the UWA channel impulse response function with the delay N_d given in terms of the symbol intervals, and $z(t)$ is the zero-mean complex additive white Gaussian noise

(AWGN) with variance N_0. The matched filter comprises low-pass and correlation filters matched to $c(t)$ [15]. The received signal after matched filtering with the qth-matched filter is represented by the following equation:

$$y_{n,q} = \sum_{\eta=0}^{N-1} u_{n-\eta,q} h_\eta + z_{n,q}, \tag{9}$$

here

$$u_{n,q} \triangleq \int_{-\infty}^{+\infty} u(t) c_q(t - nT) dt \tag{10}$$

$$z_{n,q} \triangleq \int_{-\infty}^{+\infty} z(t) c_q(t - nT) dt. \tag{11}$$

The discrete transmit signal $u_{n,q}$ is reformulated based on (4):

$$u_{n,q} = \sum_{p=0}^{K-1} \sum_{l=0}^{2L-1} \exp(j\pi h \alpha_{n-l,p}) c(p, q; l), \tag{12}$$

where the correlation function $c(p, q; l)$ is

$$c(p, q; l) \triangleq \int_{-\infty}^{+\infty} c_p(t + lT) c_q(t) dt. \tag{13}$$

3. Proposed Algorithms

For the qth-matched filter output, the posterior probability-based symbol detection is combined with FDE, resulting in the proposed PS-FDE algorithm. Figure 3 shows that PS-FDE can be divided into three parts: FDE, information merging, and symbol decision. The output of FDE, after appropriate mapping and information separation, is decomposed into information sequences at different times. Subsequently, based on the correlation function of the CPM signal, the extracted information is delayed and merged with the current symbol. The likelihood value of the merged information is calculated and used to adjust the weights during the merging process. Finally, the received symbols are obtained through hard decisions and de-mapping of the merged information.

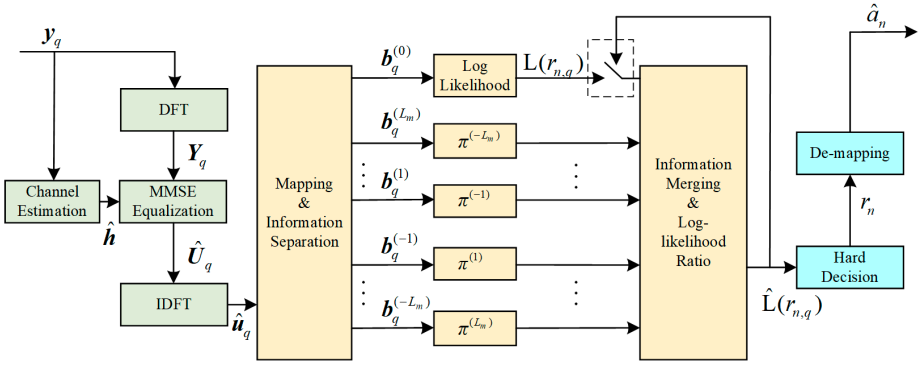

Figure 3. CPM receiver of PS-FDE.

For convenience, $c(p, q; l)$ is defined as a cyclic sequence, $c(p, q; -l) = c(p, q; 2L - l)$. The following pseudo-symbol is defined, $v_{n,p,q}^{(l)} = \exp(j\pi h \alpha_{n-l,p}) c(p, q; l)$, and $u_{n,q}$ is expressed as follows:

$$u_{n,q} = \sum_{l=1-L}^{L-1} \sum_{p=0}^{K-1} v_{n,p,q}^{(l)}, \tag{14}$$

where $l = \{1 - L, \ldots, 0, \ldots, L - 1\}$.

3.1. PS-FDE for CPM Signals

Considering the sparse property of the UWA channel, the orthogonal matching pursuit algorithm [28] is used for the channel estimation. The channel impulse response estimated by CP is expressed as $\hat{\boldsymbol{h}} = \left\{\hat{h}_0, \hat{h}_1, \ldots, \hat{h}_{N_d-1}\right\}$. According to classic FDE for CPM signal [15], the equalized signal in the frequency domain is given as follows:

$$\hat{U}_{k,q} = Y_{k,q} W_{k,q} \hat{H}_{k,q}, \tag{15}$$

where $Y_{k,q}$ and $\hat{H}_{k,q}$ are the frequency domain representations of $y_{n,q}$ and $\hat{h}_n$, respectively. MMSE equalization coefficient is expressed as

$$\hat{F}_{k,q} = \frac{\hat{H}_k^* W_{k,q}}{\left|\hat{H}_k W_{k,q}\right|^2 + N_0}, \tag{16}$$

where N_0 is the noise power spectral density. The noise-whitening filter $W_{k,q}$ is given as follows:

$$W_{k,q} = \frac{1}{\sqrt{C(p,q;k)}}, \tag{17}$$

where $C(p,q;k)$ denotes the frequency domain representations of $c(p,q;n)$.

Subsequently, symbol detection is performed on the equalized signal $\hat{u}_q$. To streamline the computation, the equalized signal is mapped according to the employed modulation scheme. The symbol information corresponding to different l values is then separated based on phase and amplitude characteristics. The mapped symbol sequences $\boldsymbol{b}_q^{(l)}$ and $\hat{\boldsymbol{v}}_{p,q}^{(l)}$ are defined, where $b_{n,q}$ is assumed to follow a Gaussian distribution. Under this assumption, the a priori probability of the lth symbol at the nth symbol interval is expressed as follows:

$$\Pr(b_{n,q}^{(l)} = \sum_{p=0}^{K-1} \hat{v}_{n,p,q}^{(l)}) = \frac{1}{\sqrt{2\pi}\sigma_q^{(l)}} \exp\left(-\frac{\left(\left|b_{n,q}^{(l)} - \sum_p \hat{v}_{n,p,q}^{(l)}\right|\right)^2}{2\left(\sigma_q^{(l)}\right)^2}\right), \tag{18}$$

where the equivalent noise variance $\sigma_q^{(l)}$ is calculated using CP because the theoretical value $\sum_p \hat{v}_{n,p,q}^{(l)}$ of CP after FDE is known at the nth symbol interval:

$$\left(\sigma_q^{(l)}\right)^2 = \frac{1}{N_c} \sum_{n=N-N_c+1}^{N} \left(\left|b_{n,q}^{(l)} - \sum_p \hat{v}_{n,p,q}^{(l)}\right|\right)^2. \tag{19}$$

$u_{n,q}$ contains information of the consecutive $l = \{1-L, \ldots, -1, 0, 1, \ldots, L-1\}$ symbols; hence, the symbol information at times $n+l$ and $n+2l$ can be delayed and merged to estimate the nth symbol. Generally, the nth symbol information carries the dominant energy within the nth symbol interval. Therefore, the initial estimated likelihood value is expressed by $b_{n,q}^{(0)}$:

$$\mathrm{L}(r_{n,q}) = \ln[\Pr(b_{n,q}^{(0)} = \textstyle\sum_p \hat{v}_{n,p,q}^{(0)})]. \tag{20}$$

During the information merging, the estimated likelihood value $\hat{\mathrm{L}}(r_{n,q})$ of the symbol is computed using a joint probability according to the symbol information of $l \neq 0$:

$$\hat{\mathrm{L}}(r_{n,q})^{(k)} = \mathrm{L}(r_{n,q}) + \sum_{l=\{1-L,\ldots,-1,1,\ldots L-1\}} \{\ln[\sum_{(\xi,\eta)\propto\sum_p \hat{v}_{n,p,q}^{(0)}} \Pr(b_{n-l,q}^{(l)} = \xi)\Pr(r_{n-2l,q} = \eta)] \times \kappa_q^{(k,l)}\} \tag{21}$$

where $\kappa_q^{(k,l)}$ is related to the noise variance $\sigma_q^{(k,l)}$ of k-times information merging and energy of $\sum_p \hat{v}_{n,p,q}^{(l)}$. According to $c(p,q;l)$, $r_{n,q} \triangleq \sum_p \hat{v}_{n,p,1}^{(0)}$ when $\left\{ b_{n-l,q}^{(l)}, r_{n-2l,q} \right\}$ satisfies the state $\{\xi, \eta\}$. This relationship is defined as $(\xi, \eta) \propto \sum_p v_{n,p,q}^{(0)}$.

The likelihood value $\mathrm{L}(r_{n,q})$ can be replaced by the estimated likelihood value $\hat{\mathrm{L}}(r_{n,q})^{(k)}$ after the information merging. The derived probabilities $\Pr(b_{n,q}^{(l)})$ and $\Pr(r_{n,q})$ are utilized to enhance symbol detection performance. The equivalent detection symbols $r_{n,q}$ are obtained from $\hat{\mathrm{L}}(r_{n,q})^{(k)}$ by hard decision. The received data $\hat{a}_n$ are given as follows [29]:

$$\hat{a}_n = \frac{1}{\pi h} \arg(r_{n,q} r_{n-1,q}^*). \tag{22}$$

Ensuring a computational stability, the algorithm is executed within the logarithmic domain as follows:

$$\widetilde{\Pr}(b_{n,q}^{(l)} = \sum_{p=0}^{K-1} \hat{v}_{n,p,q}^{(l)}) = \ln[\Pr(b_{n,q}^{(l)} = \sum_{p=0}^{K-1} \hat{v}_{n,p,q}^{(l)})]. \tag{23}$$

According to $c(p,q;l)$, an increase in l leads to a reduction in the energy ratio of the $(n+l)^{\text{th}}$ symbol information within the nth symbol interval. Consequently, the detection gain derived from $b_{n-l,q}^{(l)}$ becomes negligible. To further simplify the algorithm, only the $l = \{1 - L_m, \ldots, -1, 0, 1, \ldots L_m - 1\}$ symbol with $L_m \leq L$ is utilized in the computation of the likelihood value $\hat{\mathrm{L}}(r_{n,q})^{(k)}$. Accordingly, Equation (23) is used to reformulate the log-likelihood values $\mathrm{L}(r_{n,q})$ and $\hat{\mathrm{L}}(r_{n,q})^{(k)}$:

$$\mathrm{L}(r_{n,q}) = \ln\{\exp[\widetilde{\Pr}(b_{n,q}^{(0)} = \sum_{p=0}^{K-1} \hat{v}_{n,p,q}^{(0)})]\} \tag{24}$$

$$\hat{\mathrm{L}}(r_{n,q})^{(k)} = \mathrm{L}(r_{n,q}) \times \kappa_{p,q}^{(k,0)} + \sum_{l \neq 0} \{\ln[\sum_{(\xi,\eta) \propto \sum_p \hat{v}_{n,p,q}^{(0)}} \exp(\widetilde{\Pr}(b_{n-l,q}^{(l)} = \xi) + \widetilde{\Pr}(r_{n-2l,q} = \eta))] \times \kappa_{p,q}^{(k,l)}\} \tag{25}$$

3.2. PS-FDE for Binary CPM Signals

The overarching discourse on PS-FDE is extended to encompass a binary CPM signal with a 1/2 modulation index [29]. The signal is approximated as the summation of a single PAM signal following Laurent decomposition. Consequently, the soft symbol output obtained from FDE is transformed through the following mapping:

$$\hat{\boldsymbol{b}} = \boldsymbol{b} \exp(j\frac{\pi}{2}(n+1)), \tag{26}$$

$$\hat{\boldsymbol{v}} = \boldsymbol{v} \exp(j\frac{\pi}{2}(n+1)), \tag{27}$$

where $\boldsymbol{b}$ is the equalized signal after FDE, $\hat{\boldsymbol{b}}$ is the mapped symbol, and $\hat{\boldsymbol{v}}$ is the mapped pseudo-symbol with a different l.

The information in $\hat{\boldsymbol{b}}$ are separated into real ($\mathrm{Re}(\boldsymbol{b})$) and imaginary ($\mathrm{Im}(\boldsymbol{b})$) parts. The $\mathrm{Re}(\boldsymbol{b})$ corresponds to the information set of the $(n+l)^{\text{th}}$ symbol when l is odd, whereas the $\mathrm{Im}(\boldsymbol{b})$ corresponds to the information set of the $(n+l)^{\text{th}}$ symbol when l is even. The symbol information associated with the nth interval primarily dominates the energy within

that interval and $\mathrm{Re}(\hat{b}_n^{(0)}) \in \{\pm 1\}$ after normalization. Consequently, the initial estimated log-likelihood ratio $\mathrm{LLR}(r_n)$ is formulated as follows:

$$\mathrm{LLR}(r_n) = \ln\{\frac{\exp(\widetilde{\Pr}(\mathrm{Re}(b_n) = 1))}{\exp(\widetilde{\Pr}(\mathrm{Re}(b_n) = -1))}\}. \tag{28}$$

The estimated $\mathrm{LLR}(r_n)$ after the information merging is expressed as follows:

$$\begin{aligned}\mathrm{LLR}(r_n)^{(k)} &= \kappa^{(k)} \times \ln\{\frac{\exp(\widetilde{\Pr}(\mathrm{Re}(b_n) = 1 + \sum\limits_{l\in\mathrm{even}} A_n^{(l)}))}{\exp(\widetilde{\Pr}(\mathrm{Re}(b_n) = -1 + \sum\limits_{l\in\mathrm{even}} A_n^{(l)}))}\} \\ &+ \sum_{l\in\mathrm{odd}} [\kappa^{(l)} \times \ln \frac{\sum\limits_{(\xi,\eta)\propto\{1\}} \exp(\widetilde{\Pr}(\mathrm{Re}(b_{n-2l}) = \xi) + \widetilde{\Pr}(\mathrm{Im}(b_{n-l})g_{n-l} = \eta))}{\sum\limits_{(\xi,\eta)\propto\{-1\}} \exp(\widetilde{\Pr}(\mathrm{Re}(b_{n-2l}) = \xi) + \widetilde{\Pr}(\mathrm{Im}(b_{n-l}) = \eta))}]\end{aligned}, \tag{29}$$

where $l = \{1 - L_m, \ldots, -1, 1, \ldots L_m - 1\}$. If $\boldsymbol{b}$ follows a Gaussian distribution, the first term of (29) is rewritten as follows:

$$\ln \frac{\exp[\widetilde{\Pr}(\mathrm{Re}(b_n) = 1 + \sum_{l\in\mathrm{even}} A_n^{(l)})]}{\exp[\widetilde{\Pr}(\mathrm{Re}(b_n) = -1 + \sum_{l\in\mathrm{even}} A_n^{(l)})]} = \ln \frac{\exp[\widetilde{\Pr}(\mathrm{Re}(b_n) = 1)]}{\exp[\widetilde{\Pr}(\mathrm{Re}(b_n) = -1)]} - \sum_{l\in\mathrm{even}} (\frac{2A_n^{(l)}}{(\sigma^{(0)})^2}) \tag{30}$$

where $A_n^{(l)}$ is computed according to $\mathrm{LLR}(r_{n-l})$:

$$A_n^{(l)} = c(0, 0; l) \times [\Pr(r_{n-l} = 1) - \frac{1}{2}]. \tag{31}$$

The received data $\hat{\boldsymbol{a}}$ are obtained by

$$\hat{a}_n = -r_n r_{n-1}. \tag{32}$$

3.3. Computational Complexity

The posterior probability-based detection, Viterbi detection, and simple phase detection all rely on the soft information output from FDE; therefore, this section only compares the complexities of these three symbol detection algorithms. Table 1 displays the complexities of the three symbol detection methods, with Viterbi detection exhibiting extremely high complexity.

Table 1. Computational complexity of different symbol detection.

Symbol Detection	Computational Complexity
simple phase detection	$O(MN_m)$
posterior probability-based detection	$O(MN_m) + O(L_m MN_m) + O(mL_m MN_m)$
Viterbi detection	$O(PNM^L)$

Note: N_m represents the length of the information sequence, while M, P, L_m, and m denote the modulation order, the denominator of the modulation index, the simplified memory length of CPM, and the number of information merging, respectively.

Compared to the simple phase detection algorithm proposed by Darsena et al. [29], posterior probability-based detection requires additional information merging and the calculation of log-likelihood values. However, the overall complexity is of the same order of magnitude as the simple phase detection algorithm, so the increase in complexity is limited. Moreover, due to the coding gain of the CPM signal, the posterior probability-based detection only necessitates a few instances of information merging. Simulation results indicate that, compared to simple phase detection, the posterior probability-based detection

significantly improves symbol detection performance for UWA communication with only a slight increase in complexity.

4. Numerical Simulation

Numerical simulations were conducted to evaluate the performance of PS-FDE when applied to MSK and GMSK, comparing it with traditional FDE employing simple phase detection [15]. The system parameters used in the simulation (Table 2) were configured as follows: a 48 kHz sampling frequency, a 6 kHz center frequency, a 2 kbps transmission rate, a 4 kHz bandwidth, a signal sequence length of 1024 bits, and a CP length of 512 bits. The designed signal sequence ensured compliance with the modulated signal phase and maintained phase continuity after CP insertion. Consequently, no additional tail symbols were required.

Table 2. System parameters.

Parameter	Value
Sampling frequency	48 kHz
Center frequency	6 kHz
Bandwidth	4 kHz
Data rate	2 kbps
Data bits	1024 bits
CP bits	512 bits

4.1. Channel Model

UWA channels are characterized by severe multipath interference and time-varying properties. This paper primarily discusses the symbol detection algorithm for CPM based on posterior probabilities in conjunction with FDE; hence, the numerical simulations only consider the multipath interference of the UWA channels. The simulations were performed over a selection of representative channels, including a typical sparse channel, denoted as ChA [15], a measured shallow-sea channel referred to as ChB, and a measured deep-sea channel designated as ChC.

Table 3 presents the channel impulse response of the sparse channel ChA, with delay values expressed in symbol intervals. The response intervals correspond to integer multiples of the symbol duration. At a transmission rate of 2 kbps, the maximum delay spread is 12.5 ms, and the majority of the channel's energy is concentrated within the first three symbol intervals.

Table 3. Delay power profiles of chA [15].

Delay	0	1	2	8	12	25
Power	0.189	0.379	0.255	0.090	0.055	0.032

ChB was obtained through a sea trial conducted over a communication distance of approximately 5.3 km in a trial area with a water depth of around 163 m. The transmitter was deployed at a depth of 80 m, and the receiver was positioned at approximately 97 m. The measured channel response was derived from a transmitted 4–8 kHz chirp signal. Figure 4a illustrates the normalized time–domain response waveform of the measured channel after applying a 4–8 kHz bandpass filter, while Figure 4b shows the corresponding normalized frequency–domain response. The principal energy of ChB was highly concentrated, with a maximum delay spread of approximately 25 ms.

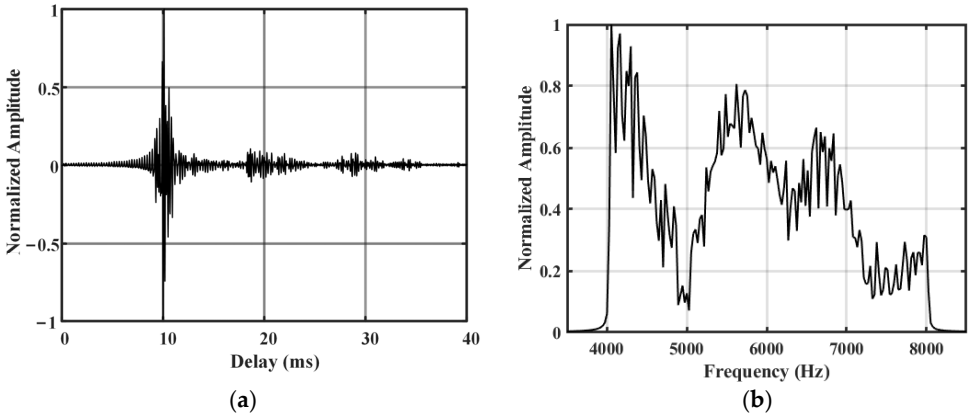

(**a**) (**b**)

Figure 4. Measured shallow-sea channel ChB (4–8 kHz bandpass filtration): (**a**) time domain; (**b**) frequency domain.

ChC was obtained through a sea trial conducted over a communication distance of approximately 10 km in a trial area with a water depth of around 3700 m. The transmitter was located at a depth of 50 m, and the receiver was positioned at approximately 3505 m. The channel response was derived from a transmitted 4–8 kHz chirp signal. Figure 5a presents the normalized time–domain response waveform of the measured channel after applying a 4–8 kHz bandpass filter, while Figure 5b depicts the corresponding normalized frequency–domain response. A notable characteristic of ChC is that its primary energy is distributed across four distinct clusters, with a maximum delay spread of approximately 120 ms.

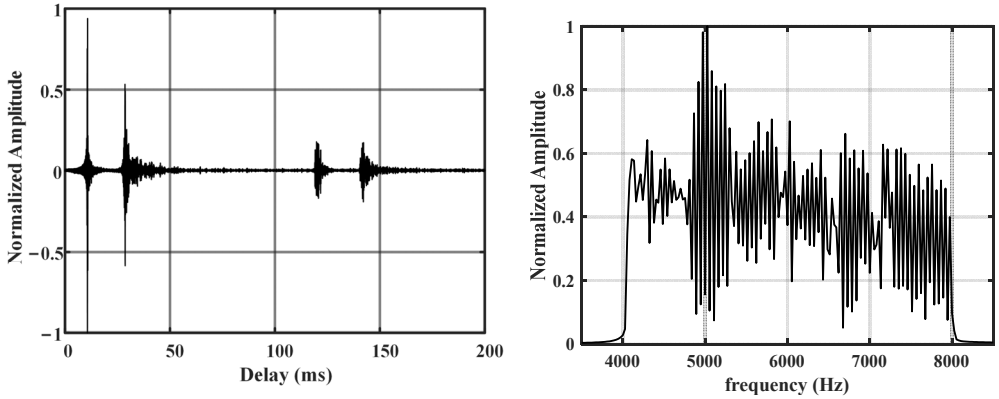

(**a**) (**b**)

Figure 5. Measured deep-sea channel ChC (4–8 kHz bandpass filtration): (**a**) time domain; (**b**) frequency domain.

4.2. Minimum Shift Keying

MSK is a distinctive form of CPM signal characterized by a 1/2 modulation index and a memory length of $L = 2$. Through Laurent decomposition, the correlation function is expressed as $c(0,0;l) \triangleq (1, 1/\pi, 0, \ldots, 0, 1/\pi)$. Then,

$$c_0(t) = \begin{cases} \sin \frac{\pi t}{2T}, & 0 \le t \le 2T \\ 0, & \text{else} \end{cases}. \tag{33}$$

If $L_m = 1$, then $\mathrm{LLR}(r_n)$ is given as

$$\begin{aligned}\mathrm{LLR}(r_n)^{(k)} &= \ln\{\frac{\exp(\widetilde{\Pr}(\mathrm{Re}(b_n)=1))}{\exp(\widetilde{\Pr}(\mathrm{Re}(b_n)=-1))}\}\times\kappa^{(k,0)} \\ &+\ln\{\frac{\sum\limits_{(\xi,\eta)\propto\{1\}}\exp(\widetilde{\Pr}(\mathrm{Re}(b_{n-2})=\xi)+\widetilde{\Pr}(\mathrm{Im}(b_{n-1})=\eta))}{\sum\limits_{(\xi,\eta)\propto\{-1\}}\exp(\widetilde{\Pr}(\mathrm{Re}(b_{n-2})=\xi)+\widetilde{\Pr}(\mathrm{Im}(b_{n-1})=\eta))}\}\times\kappa^{(k,1)} \\ &+\ln\{\frac{\sum\limits_{(\xi,\eta)\propto\{1\}}\exp(\widetilde{\Pr}(\mathrm{Re}(b_{n+2})=\xi)+\widetilde{\Pr}(\mathrm{Im}(b_{n+1})=\eta))}{\sum\limits_{(\xi,\eta)\propto\{-1\}}\exp(\widetilde{\Pr}(\mathrm{Re}(b_{n+2})=\xi)+\widetilde{\Pr}(\mathrm{Im}(b_{n+1})=\eta))}\}\times\kappa^{(k,-1)}\end{aligned}, \quad (34)$$

where the weight coefficients are $\kappa^{(k,0)} \triangleq 2E(\mathrm{Re}(b_n))/\sigma^{(k,0)}$,$\kappa^{(k,1)} = \kappa^{(k,-1)} \triangleq E(\mathrm{Im}(b_n))/\sigma^{(k,1)}$. Table 4 presents the state transitions to different l with normalization.

Table 4. State transition relations.

State		$a_n = 1$		$a_n = -1$	
$l = 1$	Ξ	1	-1	1	-1
	H	0	-1	1	0
$l = -1$	Ξ	1	-1	1	-1
	H	0	1	-1	0

Figure 6 presents the simulation results of the MSK signal over channels ChA, ChB, and ChC. The dotted line represents the theoretical bit error rate (BER) of the MSK signal in an AWGN channel, while the black line illustrates the BER performance of traditional FDE with simple phase detection [17]. The red, green, and blue curves correspond to the BER of PS-FDE for $k = 1$, $k = 2$, and $k = 3$, respectively.

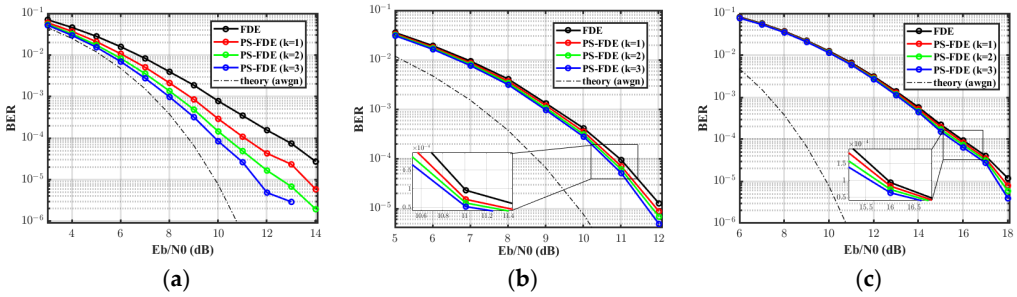

(**a**) (**b**) (**c**)

Figure 6. BER for MSK with PS-FDE: (**a**) ChA; (**b**) ChB; (**c**) ChC.

Figure 6a shows the performance of PS-FDE over ChA. During symbol detection, the first two information merges (i.e., $k = 1$ and $k = 2$) can significantly enhance performance. At BER = 10^{-4}, $k = 1$ and $k = 2$ improved the performance by 0.6 and 0.4 dB, respectively, compared with the traditional FDE [15]. Compared to the first two information merges, the third merging ($k = 3$) exhibited a modest performance enhancement of approximately 0.2 dB.

As illustrated in Figure 6b, for ChB, the BER of the MSK signal exhibited a decreasing trend as the number of information merges increased. At BER = 10^{-4}, the performance of FDE was 11 dB, while PS-FDE outperformed FDE by 0.1 dB, 0.15 dB, and 0.2 dB after the first, second, and third information merging, respectively. Figure 6c presents the results for ChC, where the performance of PS-FDE after three iterations of information merging showed improvements of 0.1 dB, 0.25 dB, and 0.45 dB, respectively, compared with the FDE performance.

The simulations conducted across the three channels consistently demonstrated that the first two iterations of information merging resulted in a significant performance improvement, whereas the third iteration exhibited a comparatively smaller performance gain.

4.3. Gaussian Minimum Shift Keying

A GMSK signal featuring a memory length of L = 3 and a bandwidth–time product of 0.3 was employed. The correlation function is represented as follows with Laurent decomposition: $c(0,0;l) = \{1, 0.447, 0.028, 8.4\times10^{-5}, \ldots, 8.4\times10^{-5}, 0.028, 0.447\}$ Then,

$$c_0(t) = \begin{cases} \sin(\pi q(t)), & 0 \le t \le LT \\ \cos(\pi q(t-LT)), & LT \le t \le 2LT \\ 0, & \text{else} \end{cases}, \tag{35}$$

here

$$q(t) = \begin{cases} 1/2, & t > LT \\ \int_0^t g(\tau)d\tau, & 0 \le t \le LT \\ 0, & t < 0 \end{cases}, \tag{36}$$

$$g(\tau) = \frac{1}{2T}\begin{cases} \frac{Q[2\pi B(\tau-\frac{T}{2})]-Q[2\pi B(\tau+\frac{T}{2})]}{\sqrt{ln2}}, & 0 \le \tau \le LT \\ 0, \quad \text{else} \end{cases}. \tag{37}$$

where $Q(x)$ is a complementary error function.

The detection gain is low because the symbol energy of $l = \pm4$ is low. Thus, $L_m = 3$ was used to calculate the $\mathrm{LLR}(r_n)$ from (29):

$$\begin{aligned} \mathrm{LLR}(r_n)^{(k)} &= \ln\{\frac{\exp(\widetilde{\Pr}(\mathrm{Re}(b_n)=1))}{\exp(\widetilde{\Pr}(\mathrm{Re}(b_n)=-1))}\}\times\kappa^{(k,0)} - \frac{2(A_n^{(2)}+A_n^{(-2)})}{(\sigma^{(0)})^2}\times\kappa^{(k,0)} \\ &+ \ln\{\frac{\sum_{(\xi,\eta)\propto\{1\}}\exp(\widetilde{\Pr}(\mathrm{Re}(b_{n-2})=\xi)+\widetilde{\Pr}(\mathrm{Im}(b_{n-1})=\eta))}{\sum_{(\xi,\eta)\propto\{-1\}}\exp(\widetilde{\Pr}(\mathrm{Re}(b_{n-2})=\xi)+\widetilde{\Pr}(\mathrm{Im}(b_{n-1})=\eta))}\}\times\kappa^{(k,1)} \\ &+ \ln\{\frac{\sum_{(\xi,\eta)\propto\{1\}}\exp(\widetilde{\Pr}(\mathrm{Re}(b_{n+2})=\xi)+\widetilde{\Pr}(\mathrm{Im}(b_{n+1})=\eta))}{\sum_{(\xi,\eta)\propto\{-1\}}\exp(\widetilde{\Pr}(\mathrm{Re}(b_{n+2})=\xi)+\widetilde{\Pr}(\mathrm{Im}(b_{n+1})=\eta))}\}\times\kappa^{(k,-1)} \end{aligned}, \tag{38}$$

where $A_n^{(l)} = c(0,0;l)\times[\Pr(\hat{u}_{n-l}=1)-1/2]$. Table 4 provides the state transitions to a different l with normalization.

Figure 7 depicts the simulation results of the GMSK signal over ChA, ChB, and ChC. The dotted line represents the theoretical value of the GMSK signal over the AWGN channel, while the black line displays the BER of traditional FDE with simple phase detection [17]. The red, green, and blue curves correspond to the BER of PS-FDE after $k = 1$, $k = 2$, and $k = 3$ information merging, respectively.

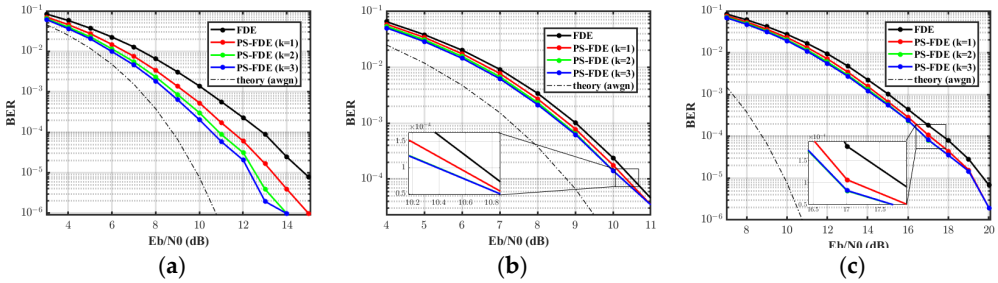

Figure 7. BER for GMSK with PS-FDE: (**a**) ChA; (**b**) ChB; (**c**) ChC.

Figure 7a shows the simulation results of the GMSK signal within ChA. At a BER of 10^{-4}, the performance of FDE was 13 dB, while PS-FDE, after three iterations of information merging, exhibited improvements of 1.4 dB, 2 dB, and 2.3 dB, respectively. Figure 7b presents the BER curve within ChB. At a BER of 10^{-4}, FDE performance yielded 10.5 dB, whereas that of PS-FDE following three iterations of information merging improved by 0.2, 0.3, and 0.3 dB, respectively. Note the similarity of the performance in the third information merging to that in the second. Figure 7c displays the BER curve within ChC. At a BER of 10^{-4}, FDE performance was 11.2 dB, whereas PS-FDE resulted in enhancements of 0.3, 0.45, and 0.45 dB, respectively. Overall, the first two iterations of information merging resulted in significant improvements in symbol detection performance, whereas the third iteration provided only a marginal enhancement in BER performance.

The simulations conducted on the aforementioned channels with MSK and GMSK signals effectively validated the performance of PS-FDE. PS-FDE achieved substantial improvements during the first two iterations of the information merging, while the incremental gains became significantly limited in the third iteration. Given that the information merging of PS-FDE was predicated on the memory inherent within CPM signals, the information provided by CPM in the information merging gradually converged as the iteration count increased; the error correction capability also gradually weakened. The inherent coding gain of CPM signals was comparably lower than the traditional channel coding, limiting the extent of the performance augmentation. Moreover, tailoring a suitable κ for the information merging necessitates due consideration that corresponds to the diverse CPM signals and the distinct channel structures at play.

5. Sea Trial

A sea trial of MSK UWA communication was conducted during winter in the South China Sea to verify the proposed algorithms. Figure 8 shows that the average depth of the test area was 208 m, and the communication distance was approximately 5.3 km. A transducer operating at an 80 m depth transmitted MSK signal at three distinct source levels of 196, 190, and 184 dB. The hydrophone positioned at a 97 m depth received the signal.

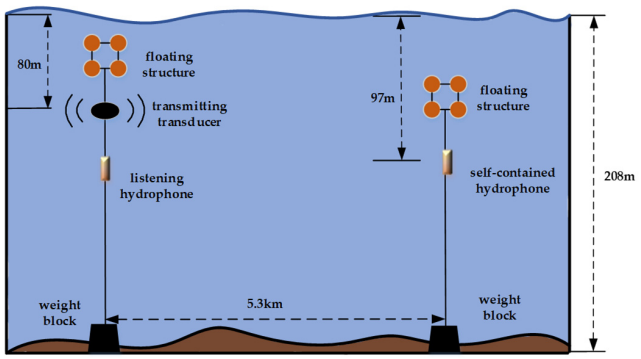

Figure 8. Sea trial program.

Figure 9 presents the measured structure of the UWA channel, which was obtained by applying the OMP algorithm to the MSK signal. The maximum delay of the channels was approximately 23 ms, which could be divided into four multiple-path clusters. Throughout the course of the sea trial, 210 groups of MSK signals were transmitted at 6 kHz center frequency, 4–8 kHz transducer bandwidth, 2 kbps communication rate, and 256 bits per frame transmission information sequence. FDE and PS-FDE were used to receive the MSK signal, wherein the FDE error bit was equivalent to that of the PS-FDE at $k = 0$.

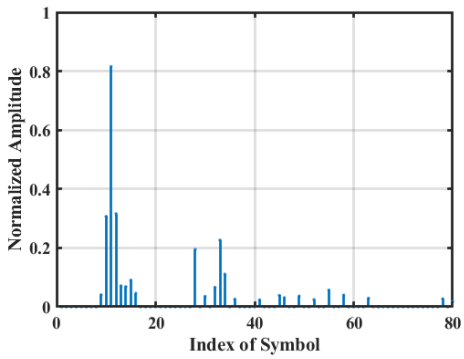

Figure 9. Measured channel of MSK signal by OMP.

Table 5 presents the number of bit errors in the received signal at different signal-to-noise ratios (SNRs) within the 4–8 kHz bandwidth. Variations in source levels and propagation losses during UWA communication led to differences in the computed SNR values. The BER of different algorithms exhibited a significant decline as SNR increased. At $k = 0$, the performance of PS-FDE was equivalent to that of traditional FDE (FDE with simple phase detection). Compared with traditional FDE, PS-FDE reduced the number of bit errors by 10, 34, and 44 at $k = 1$, $k = 2$, and $k = 3$, respectively, demonstrating its effectiveness. As the number of information merging iterations k increases, the amount of effective symbol information obtained in the final merging process decreases. Consequently, the detection gain approached saturation, leading to a gradual reduction in performance improvement.

Table 5. Number of error bits of received signal frames in different received SNRS.

SNR (dB)	Number of Frames	Error Bit of the FDE	Error Bit of the PS-FDE			
			$k = 0$	$k = 1$	$k = 2$	$k = 3$
5–10	22	212	212	206	188	182
10–15	52	58	58	56	52	48
15–20	72	8	8	6	4	4
>20	64	0	0	0	0	0
Total	210	278	278	268	244	234

6. Conclusions

CPM was applied to improve the bandwidth and the power efficiency of UWA communication, and PS-FDE was proposed to further improve CPM signal detection performance compared with the traditional FDE. It has a lower complexity than the Viterbi algorithm and uses simple phase detection to extract preliminary information. Combined with the correlation function of CPM, PS-FDE effectively harnesses the inherent coding gain within CPM, ultimately improving the symbol detection performance. Simulations were conducted using MSK and GMSK signals over UWA channels, and the results show that PS-FDE significantly improves detection performance after 2–3 information mergings, compared with that of FDE [15]. The performance improvement for MSK signals ranged from 0.2 to 1.2 dB under different channel conditions, while for GMSK signals, it ranged

from 0.3 to 2.3 dB. The results of the sea trial conducted to prove the effectiveness of the algorithms revealed that compared with that of FDE [15], the BER of PS-FDE exhibited a 15.83% reduction after the third information merging.

Due to the time-varying nature of UWA channels, the FDE and OMP channel estimation algorithms used in this paper struggle to effectively track channel variations. Consequently, the BER of sea trials is relatively high. Due to the high compatibility of the symbol detection algorithm proposed in this paper with channel equalization, future work will consider integrating this symbol detection algorithm with channel equalization algorithms capable of tracking time-varying channels to enhance the capability to combat time-varying UWA channels.

Author Contributions: Conceptualization, R.H. and N.J.; methodology, R.H.; software, Y.L. and J.H.; validation, N.J.; formal analysis, R.H.; investigation, R.H.; resources, S.G.; data curation, S.Q.; writing—original draft preparation, R.H.; writing—review and editing, R.H. and N.J.; visualization, Y.L.; supervision, J.H.; project administration, S.G.; funding acquisition, N.J. and S.G. All authors have read and agreed to the published version of the manuscript.

Funding: This research was funded by the Youth Innovation Promotion Association, Chinese Academy of Sciences, grant number 2020024.

Data Availability Statement: The original contributions presented in this study are included in the article. Further inquiries can be directed to the corresponding author.

Acknowledgments: Thanks to the personnel involved in the sea trial and the research vessel "Shiyan 1" for their contributions to data acquisition for the project.

Conflicts of Interest: The authors declare no conflicts of interest.

Abbreviations

Abbreviation	Full Term
UWA	Underwater acoustic
CPM	Continuous phase modulation
FDE	Frequency domain equalization
PS-FDE	Posterior probability-based symbol detection with FDE
MSK	Minimum shift keying
GMSK	Gaussian MSK
PSK	Phase-shift keying
CP	Cyclic prefix
AWGN	Additive white Gaussian noise
MMSE	Minimum mean square error
LLR	Log-likelihood ratio
SNR	Signal-to-noise ratio
BER	Bit error rate
OMP	Orthogonal matching pursuit

References

1. Tong, F.; Zhou, Y.; Chen, D.; Li, J.; Zhang, X. Advances and trends of underwater acoustic communication technology for heterogeneous unmanned underwater vehicles. *J. Harbin Eng. Univ.* **2023**, *44*, 1963–1976.
2. Lu, M.; Mengyao, L.; Songzuo, L. A multi-beam space diversity method for long-range underwater acoustic OFDM communication in deep water. *ACTA Acust.* **2022**, *47*, 579–590.
3. Zhi, S.; Hongzhi, G.; Akyildiz, I.F. High-Data-Rate Long-Range Underwater Communications via Acoustic Reconfigurable Intelligent Surfaces. *IEEE Commun. Mag.* **2022**, *60*, 96–102.
4. Aulin, T.; Sundberg, C. Continuous phase modulation—Part I: Full response signalling. *IEEE Trans. Commun.* **1981**, *29*, 196–209. [CrossRef]

5. Aulin, T.; Rydbeck, N.; Sundberg, C.-E. Continuous phase modulation-part II: Partial response signalling. *IEEE Trans. Commun.* **1981**, *29*, 210–225. [CrossRef]
6. Xue, R.; Wang, T. Adaptive Parameter Selection in the Simultaneous Transmission of CPM Communication and PN Ranging. *IEEE Trans. Aerosp. Electron. Syst.* **2023**, *59*, 1590–1597. [CrossRef]
7. Wen, Y.; Yang, F. Free Space Optical Integrated Sensing and Communication Based on LFM and CPM. *IEEE Commun. Lett.* **2024**, *28*, 43–47. [CrossRef]
8. Arabian, F.; Rice, M. On Polarization, Combining, and Equalization in Aeronautical Mobile Telemetry. *IEEE Trans. Aerosp. Electron. Syst.* **2022**, *58*, 3601–3612. [CrossRef]
9. Yang, T.C. Measurements of temporal coherence of sound transmissions through shallow water. *J. Acoust. Soc. Am.* **2006**, *120*, 2595–2614. [CrossRef]
10. Jobst, W.; Zabalgogeazcoa, X. Coherence estimates for signals propagated through acoustic channels with multiple paths. *J. Acoust. Soc. Am.* **1979**, *65*, 622–630. [CrossRef]
11. Yiin, L.; Stuber, G.L. MLSE and soft-output equalization for trellis-Coded continuous phase modulation. *IEEE Trans. Commun.* **1997**, *45*, 651–659. [CrossRef]
12. Duel-Hallen, A.; Heegard, C. Delayed decision-feedback sequence estimation. *IEEE Trans. Commun.* **1989**, *37*, 428–436. [CrossRef]
13. Laurent, P. Exact and approximate construction of digital phase modulations by superposition of amplitude modulated pulses (AMP). *IEEE Trans. Commun.* **1986**, *34*, 150–160. [CrossRef]
14. Mengali, U.; Morelli, M. Decomposition of M-ary CPM signals into PAM waveforms. *IEEE Trans. Inf. Theory* **1995**, *41*, 1265–1275. [CrossRef]
15. Tan, J.; Stuber, G.L. Frequency-domain equalization for continuous phase modulation. *IEEE Trans. Wirel. Commun.* **2005**, *4*, 2479–2490. [CrossRef]
16. Pancaldi, F.; Vitetta, G.M. Equalization algorithms in the frequency domain for continuous phase modulations. *IEEE Trans. Commun.* **2006**, *54*, 648–658. [CrossRef]
17. Park, H.; Heath, R.W.; Rappaport, T.S. Frequency-domain channel estimation and equalization for continuous-phase modulations with superimposed pilot sequences. *IEEE Trans. Veh. Technol.* **2009**, *58*, 4903–4908. [CrossRef]
18. Van Thillo, W.; Horlin, F.; Nsenga, J.; Ramon, V.; Bourdoux, A.; Lauwereins, R. Low-complexity linear frequency domain equalization for continuous phase modulation. *IEEE Trans. Wirel. Commun.* **2009**, *8*, 1435–1445. [CrossRef]
19. Saleem, S.; Stüber, G.L. Frequency-domain equalization techniques for multi-h continuous phase modulation. *IEEE Trans. Commun.* **2014**, *62*, 1818–1829. [CrossRef]
20. Chayot, R.; Thomas, N.; Poulliat, C.; Boucheret, M.L.; Lesthievent, G.; Van Wambeke, N. A new exact low-complexity MMSE equalizer for continuous phase modulation. *IEEE Commun. Lett.* **2018**, *22*, 2218–2221. [CrossRef]
21. Rice, M.; Perrins, E. A comparison of frequency-domain equalization techniques in aeronautical telemetry. In Proceedings of the 9th Latin American Conference on Communications (LATINCOM), Guatemala City, Guatemala, 8–10 November 2017; pp. 1–6.
22. Van Thillo, W.; Horlin, F.; Ramon, V.; Bourdoux, A.; Lauwereins, R. Novel block constructions using an intrafix for CPM with frequency domain equalization. *IEEE Trans. Wirel. Commun.* **2010**, *9*, 951–955. [CrossRef]
23. Van Thillo, W.; Ramon, V.; Bourdoux, A.; Horlin, F.; Sleurs, K.; Lauwereins, R. Training sequence versus cyclic prefix for CPM with frequency domain equalization. In Proceedings of the GLOBECOM IEEE Global Telecommunications Conference, Honolulu, HI, USA, 30 November–4 December 2009; pp. 1–5.
24. Othman, R.; Louët, Y.; Skrzypczak, A. Joint channel estimation and detection of SOQPSK using the PAM decomposition. In Proceedings of the 25th International Conference on Telecommunications (ICT), Saint-Malo, France, 26–28 June 2018; pp. 154–158.
25. Brown, C.; Vigneron, P.J. Channel estimation and equalisation for single carrier continuous phase modulation. In Proceedings of the Military Communications Conference, Baltimore, MD, USA, 7–10 November 2011; pp. 334–340.
26. Ozgul, B.; Koca, M.; Delic, H. Double turbo equalization of continuous phase modulation with frequency domain processing. *IEEE Trans. Commun.* **2009**, *57*, 423–429. [CrossRef]
27. Güntürkün, U.; Vandendorpe, L. Low-Complexity LMMSE–SIC turbo receiver for continuous phase modulation, based on a multiaccess–multipath analogy. *IEEE Trans. Commun.* **2020**, *68*, 7672–7686. [CrossRef]
28. Tropp, J.A.; Gilbert, A.C. Signal recovery from random measurements via orthogonal matching pursuit. *IEEE Trans. Inf. Theory* **2007**, *53*, 4655–4666. [CrossRef]
29. Darsena, D.; Gelli, G.; Iudice, I.; Verde, F. Equalization techniques of control and non-payload communication links for unmanned aerial vehicles. *IEEE Access* **2018**, *6*, 4485–4496. [CrossRef]

Disclaimer/Publisher's Note: The statements, opinions and data contained in all publications are solely those of the individual author(s) and contributor(s) and not of MDPI and/or the editor(s). MDPI and/or the editor(s) disclaim responsibility for any injury to people or property resulting from any ideas, methods, instructions or products referred to in the content.